16th World Conference on Earthquake Engineering, 16WCEE 2017
Santiago Chile, January 9th to 13th 2017
Paper N° 221 (Abstract ID)
Registration Code: S-C1463211996

GREEN'S FUNCTION DATABASE AND DETAILED GROUND MOTION PREDICTION FOR CENTRAL JAPAN BASED ON THE RECIPROCITY THEOREM

T. Hirai[(1)], N. Fukuwa[(2)]

[(1)] *Assistant Professor, Graduate School of Environmental Studies, Nagoya University, hirai.takashi@nagoya-u.jp*
[(2)] *Professor, Disaster Mitigation Research Center, Nagoya University, fukuwa@sharaku.nuac.nagoya-u.ac.jp*

Abstract

Detailed prediction of ground motion is important in the design of high-rise, base-isolated, and other key buildings. In general, the predominant period of ground motion is considered to be constant at each site. However, some recent studies have reported that the predominant period of observed ground motion can vary according to the source direction at sites on sedimentary basins. Therefore, detailed ground motion prediction with waveforms should be advanced for sites containing the types of buildings described above.

The waveform of long-period ground motion is often predicted using the finite difference method, since the complicated soil structure of a sedimentary basin can be considered with this method. However, ground motion calculations using the finite difference method require large amounts of computational resources and time. If many possible earthquakes are assumed around an important site, it is very expensive to predict the long-period ground motion.

In this study, we propose an efficient method for predicting long-period ground motions due to many possible earthquakes for a specific site. In this method, the Green's functions of the ground motions are calculated using the finite difference method based on the reciprocity theorem. According to this theorem, the displacement at the site due to a double couple force at the source equals the strain at the source due to a single force at the site. By using the reciprocity of Green's functions, the computational cost of obtaining a complete set of Green's functions can be dramatically reduced. Once the Green's functions representing the displacement at the site due to every element fault have been compiled in a database, the ground motions at the site due to earthquakes with arbitrary mechanisms can be easily predicted by superposing Green's functions.

We apply above scheme to predict ground motions at several important sites in central Japan. As a result, the ground motions at the sites due to several cases of future earthquakes can be calculated efficiently. In addition, our scheme is useful for discussing the behavior of ground motion and the impact on the buildings in relation to seismic mechanisms.

Keywords: Long-period ground motion; Green's function; Reciprocity theorem; Finite difference method

1. Introduction

Many major earthquakes have occurred in and around Japan. The anticipated Nankai Trough Earthquake may well be the most hazardous earthquake in Japan, with a magnitude M_w that may be as high as 9.1. Such large earthquakes cause long-duration, long-period ground motion.

In order to discuss long-period ground motion, the effect of irregular soil structure, such as that of a sedimentary basin, should be taken into account. Trifunac and Hudson [1], Boore [2], and Bouchon [3] analyzed the strong ground motion record at the Pacoima Dam during the San Fernando Earthquake (1971), considering the effect of the irregularity of the soil structure around the dam. Sánchez-Sesma et al. [4] analyzed the long-duration, long-period ground motion due to the Mexico Earthquake (1985) and concluded that the component with a period of 2–3 s was caused by the soil structure of a sedimentary basin. In Japan, strong long-period ground motion was observed in the Tokachi-Oki Earthquake (1968). Recently, in the case of the Tohoku-Oki Earthquake (2011), a large response was recorded at the top of a high-rise building located on the Osaka sedimentary basin [5]. The response is considered to be due to resonance between the soil and the building.

Generally, the ground motion at a site is determined by three factors: the source characteristics, the path of the seismic wave, and the effect of surface subsoil. However, the nature of long-period ground motion can vary according to the direction and depth of the hypocenter. For example, Yuzawa and Nagumo [6] revealed that the predominant period of long-period ground motion varies across the Kanto sedimentary basin, Japan. Terashima et al. [7] indicated that the predominant period of long-period ground motion at the KiK-net Konohana site (Osaka, Japan) varies according to the source direction.

There are several numerical techniques for simulating long-period ground motion, e.g., the finite element method (FEM), the spectral element method (SEM), and the finite difference method (FDM). Although complicated soil structure can be taken into account by any of these techniques, large amount of computational resources and long calculation times are required. Of these methods, FDM uses the simplest formulation and requires a relatively small amount of memory that is proportional to the number of grids. Therefore, FDM is widely used to predict the simultaneous ground motion due to huge earthquakes, e.g., to produce hazard maps.

According to the reciprocity theorem of an elastic body, the Green's function representing a site displacement due to a double couple force at the hypocenter is the same Green's function that represents the strain at the hypocenter due to a single force at the site. Combining the FDM and the reciprocity theorem, the Green's functions representing a site displacement due to all the assumed sources can be calculated simultaneously. This approach has been used previously for seismic source inversion. For example, Simuté and Fichtner [8] calculated numerous Green's function data in and around Japan based on the reciprocity theorem for seismic source inversion. However, it is less common to use the reciprocity theorem of Green's functions for ground motion prediction.

The above-mentioned scheme for predicting ground motion can be applied to the aseismic design of buildings. In the case of ground motion prediction at a specific site, a rupture scenario of the seismic fault is assumed initially. In general, several seismic-fault rupture scenarios are assumed and the ground motions are calculated for each scenario. However, to calculate long-period ground motion using the FDM would be computationally expensive because the ground motions for all rupture scenarios would have to be calculated. If the ground motion is required to be predicted at only a few sites, it is beneficial to use the reciprocity theorem to calculate the Green's functions. In this study, we develop a database that contains the Green's functions representing the ground motions at a specific site due to each element fault of the assumed seismic faults. Using the database, the ground motion at a specific site due to an arbitrary rupture scenario of the seismic fault can be calculated efficiently by superposing Green's functions. Even if detailed prediction of ground motion is not necessary, it is important for the aseismic design of buildings to evaluate the variation of the ground-motion characteristics.

2. Theory

2.1 Calculation of Green's function using reciprocity theorem

According to the theory of elasticity, the ground motion due to an earthquake is given by the following equation:

$$u_i(\boldsymbol{x},t)=\sum_{p=1}^{3}\sum_{q=1}^{3}\int_{-\infty}^{t}\int_{V}\frac{\partial G_{ip}(\boldsymbol{x},t-\tau;\boldsymbol{\xi},0)}{\partial\xi_q}m_{pq}(\boldsymbol{\xi},\tau)\,dV\,d\tau\,. \tag{1}$$

Above equation denotes the *i*-th component of the displacement at site $\boldsymbol{x}$ at time *t* due to the earthquake in the source region *V*. $\boldsymbol{\xi}$ and m_{pq} denote the position in the source region and the *pq*-component of the moment tensor, respectively. $G_{ip}(\boldsymbol{x},t-\tau;\boldsymbol{\xi},0)$ denotes the *i*-th component of the displacement at site $\boldsymbol{x}$ and at time *t* due to the impulse force along the x_p axis at the source $\boldsymbol{\xi}$ at time *t*; this is known as the Green's function. The reciprocity theorem is expressed as follows:

$$G_{ip}(\boldsymbol{x},t-\tau;\boldsymbol{\xi},0)=G_{pi}(\boldsymbol{\xi},t-\tau;\boldsymbol{x},0)\,. \tag{2}$$

Substituting Eq. (2) to Eq. (1), we obtain

$$u_i(\boldsymbol{x},t)=\sum_{p=1}^{3}\sum_{q=1}^{3}\int_{-\infty}^{t}\int_{V}\frac{\partial G_{pi}(\boldsymbol{\xi},t-\tau;\boldsymbol{x},0)}{\partial\xi_q}m_{pq}(\boldsymbol{\xi},\tau)\,dV\,d\tau\,. \tag{3}$$

Comparing Eqs. (1) and (2), the *pq*-component of the displacement gradient at source $\boldsymbol{\xi}$ due to the impulse force along the x_i axis at site $\boldsymbol{x}$ equals the *i*-th component of the displacement at site $\boldsymbol{x}$ due to the impulsive release of the *pq*-component of the moment tensor at source $\boldsymbol{\xi}$.

As discussed in Section 1, the displacement of all grids of the model is calculated simultaneously by the FDM. If there are *M* assumed earthquakes and *N* sites, all the ground motions are calculated by running the FDM simulation *M* times. In contrast, using the reciprocity theorem of Green's functions, the same results are given by running the FDM simulation 3*N* times. Once the Green's functions representing the ground motion at the site due to each element fault have been calculated, the ground motion due to a large earthquake can be constructed by superposing the Green's functions. If *N* is much smaller than *M*, the ground motions are calculated more efficiently by using the reciprocity theorem.

To calculate $\partial G_{pi}(\boldsymbol{\xi},t-\tau;\boldsymbol{x},0)/\partial\xi_q$ in Eq. (3) by the FDM, the constitutive law of an elastic body is used in this study. Assuming an isotropic homogeneous medium, the strain tensors are given as the solution of the equation

$$\begin{pmatrix}\tau_{xx}\\ \tau_{yy}\\ \tau_{zz}\\ \tau_{yz}\\ \tau_{zx}\\ \tau_{xy}\end{pmatrix}=\begin{pmatrix}\lambda+2\mu & \lambda & \lambda & 0 & 0 & 0\\ \lambda & \lambda+2\mu & \lambda & 0 & 0 & 0\\ \lambda & \lambda & \lambda+2\mu & 0 & 0 & 0\\ 0 & 0 & 0 & 2\mu & 0 & 0\\ 0 & 0 & 0 & 0 & 2\mu & 0\\ 0 & 0 & 0 & 0 & 0 & 2\mu\end{pmatrix}\begin{pmatrix}\varepsilon_{xx}\\ \varepsilon_{yy}\\ \varepsilon_{zz}\\ \varepsilon_{yz}\\ \varepsilon_{zx}\\ \varepsilon_{xy}\end{pmatrix}, \tag{4}$$

where λ and μ denote the Lamé constants. Although the displacement gradient tensor is necessary for calculating the ground motion using Eq. (3), it can be replaced by the strain tensor because the moment tensor is symmetric. Therefore, Eq. (3) is rewritten as

$$u_i(\boldsymbol{x},t)=\sum_{p=1}^{3}\sum_{q=1}^{3}\int_{-\infty}^{t}\int_V H_{ipq}(\boldsymbol{x},t-\tau;\boldsymbol{\xi},0)\,m_{pq}(\boldsymbol{\xi},\tau)\,dV\,d\tau\,, \tag{5}$$

where $H_{ipq}(\boldsymbol{x},t-\tau;\boldsymbol{\xi},0)$ is defined as

$$H_{ipq}(\boldsymbol{x},t-\tau;\boldsymbol{\xi},0)=\frac{1}{2}\left\{\frac{\partial G_{pi}(\boldsymbol{\xi},t-\tau;\boldsymbol{x},0)}{\partial\xi_q}+\frac{\partial G_{qi}(\boldsymbol{\xi},t-\tau;\boldsymbol{x},0)}{\partial\xi_p}\right\}. \tag{6}$$

The strain tensor given by Eq. (4) corresponds to Eq. (6).

2.2 Wave synthesis

In this study, the seismic fault of a large earthquake is replaced by many element faults. This technique is also used in other wave synthesis methods such as the empirical Green's function method and the stochastic Green's function method. The velocity due to an earthquake with *n* element faults is given by

$$v_i(\boldsymbol{x},t)=\sum_{j=1}^{n}\sum_{p=1}^{3}\sum_{q=1}^{3}\int_{-\infty}^{t}H_{ipq}(\boldsymbol{x},t-\tau;\boldsymbol{\xi}_j,0)\frac{M_{jpq}(\tau)}{d\tau}d\tau\,, \tag{7}$$

where $\boldsymbol{\xi}_j$ and $M_{jpq}(\tau)$ denote the position of the *j*-th element and its moment tensor function, respectively. The source time function $M_{jpq}(\tau)/d\tau$ in Eq. (7) is given as follows:

$$\frac{M_{jpq}(\tau)}{d\tau}=\left(n_{jp}v_{jq}+n_{jq}v_{jp}\right)M_{0j}\,f\left(\tau-\tau_{\mathrm{d}j}\right), \tag{8}$$

where n_j and v_j denote the unit normal vector and the unit slip vector of *j*-th element, respectively. $f(\tau)$ and τ_{d} are the source time function and the rupture time of the *j*-th element, respectively.

In this study, the source time function is defined as

$$f(t)=\omega_{\mathrm{c}}^2 te^{-\omega_{\mathrm{c}}t}\theta(t), \tag{9}$$

where $\theta(t)$ is the unit step function. The Fourier spectrum of Eq. (9) has the form of a ω^{-2} spectrum, namely

$$F(\omega)=\frac{1}{\left(1+i\dfrac{\omega}{\omega_{\mathrm{c}}}\right)^2}. \tag{10}$$

The corner angular frequency ω_{c} is estimated in this study using Boore's formulation of a circular crack [9],

$$\omega_{\mathrm{c}}=2\pi f_{\mathrm{c}}=2\pi\times 0.49V_{\mathrm{S}}\left(\frac{\Delta\sigma}{M_0}\right)^{1/3}, \tag{11}$$

where V_{S} and $\Delta\sigma$ denote the S-wave velocity and the stress drop, respectively.

3. Application to inland earthquakes

3.1 Soil structure and seismic source model

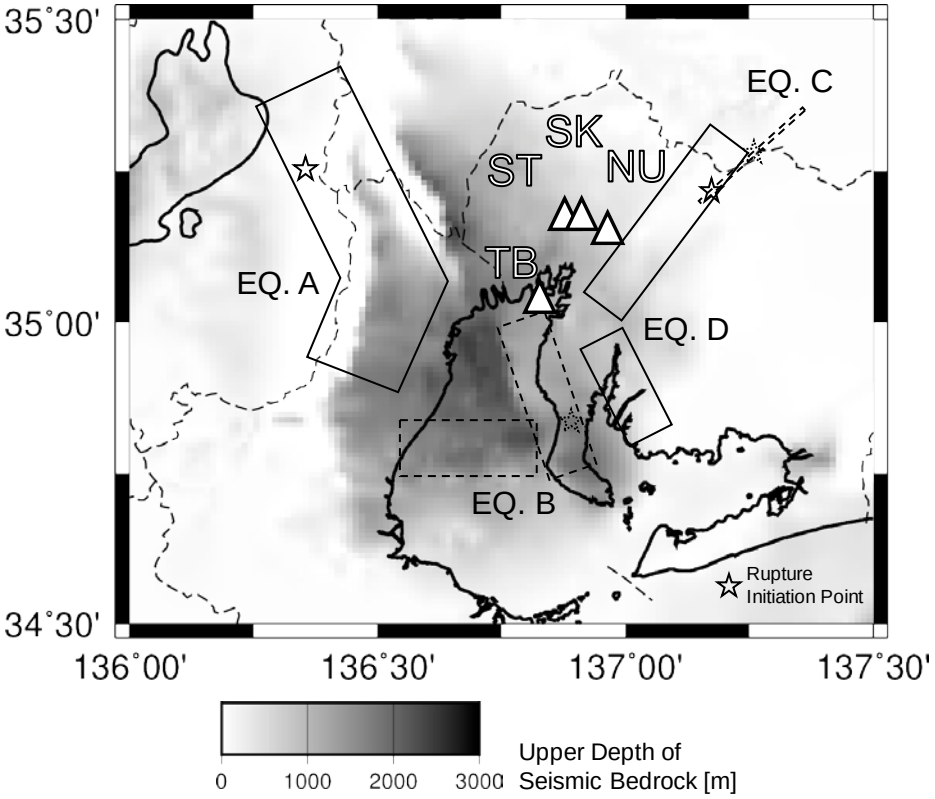

Fig. 1 – Soil structure, ground motion prediction sites, and seismic faults.

Table 1 – Details of ground motion prediction sites.

Site	Latitude [deg]	Longitude [deg]	Topography
TB	35.0330	136.8301	Reclaimed ground
ST	35.1708	136.8816	Back marsh
SK	35.1686	136.9103	Gravelly plateau
NU	35.1557	136.9686	Hill

The ground motion prediction method described in this paper is applied to inland earthquakes in and around Nagoya, central Japan.

Figure 1 shows the soil structure of the model area, the ground motion prediction sites, and the seismic faults considered. The soil structure is drawn as the upper-depth distribution of the layer with V_S = 3200 m/s. In this region, a thick sedimentary layer exists beneath the Nobi Plain. Table 1 gives the details of the ground motion prediction sites. Figure 2 shows the seismic fault models of objective earthquakes. In this study, the ground motions are predicted for these earthquakes because they are considered to cause serious damage in central Japan. The element faults shown in Fig. 2 were defined by the Japan Seismic Hazard Information Station [10]. Although several cases of the asperity distribution and the rupture initiation point were estimated for these fault models, the most intense cases of each model are used in this study, except for earthquake A. Specifically, we use case 2 for earthquake B, the unique case for earthquake C, case 6 for earthquake D, and all the cases for earthquake A.

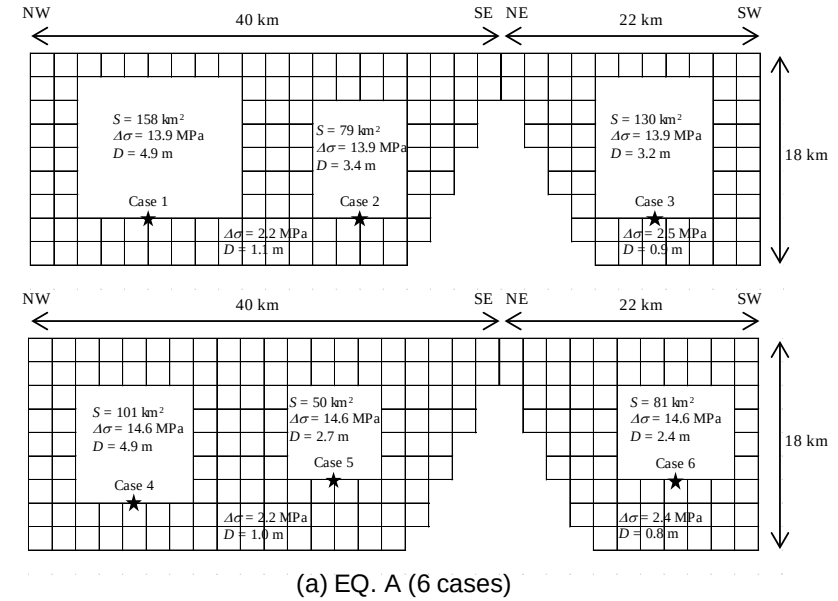

(a) EQ. A (6 cases)

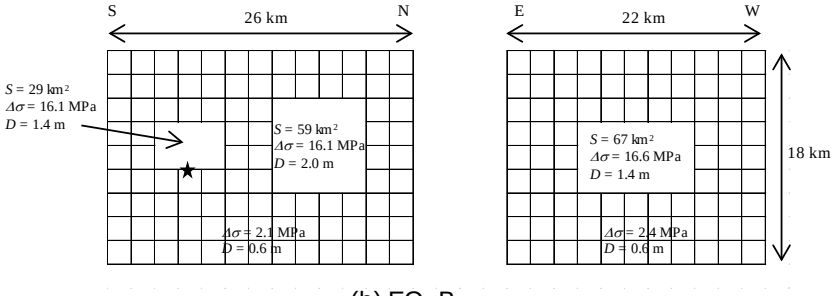

(b) EQ. B

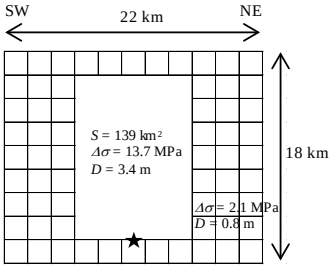

(c) EQ. C

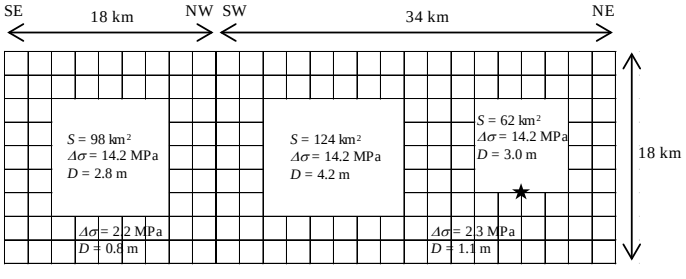

(d) EQ. D

Fig. 2 – Seismic fault models of objective earthquakes [10].

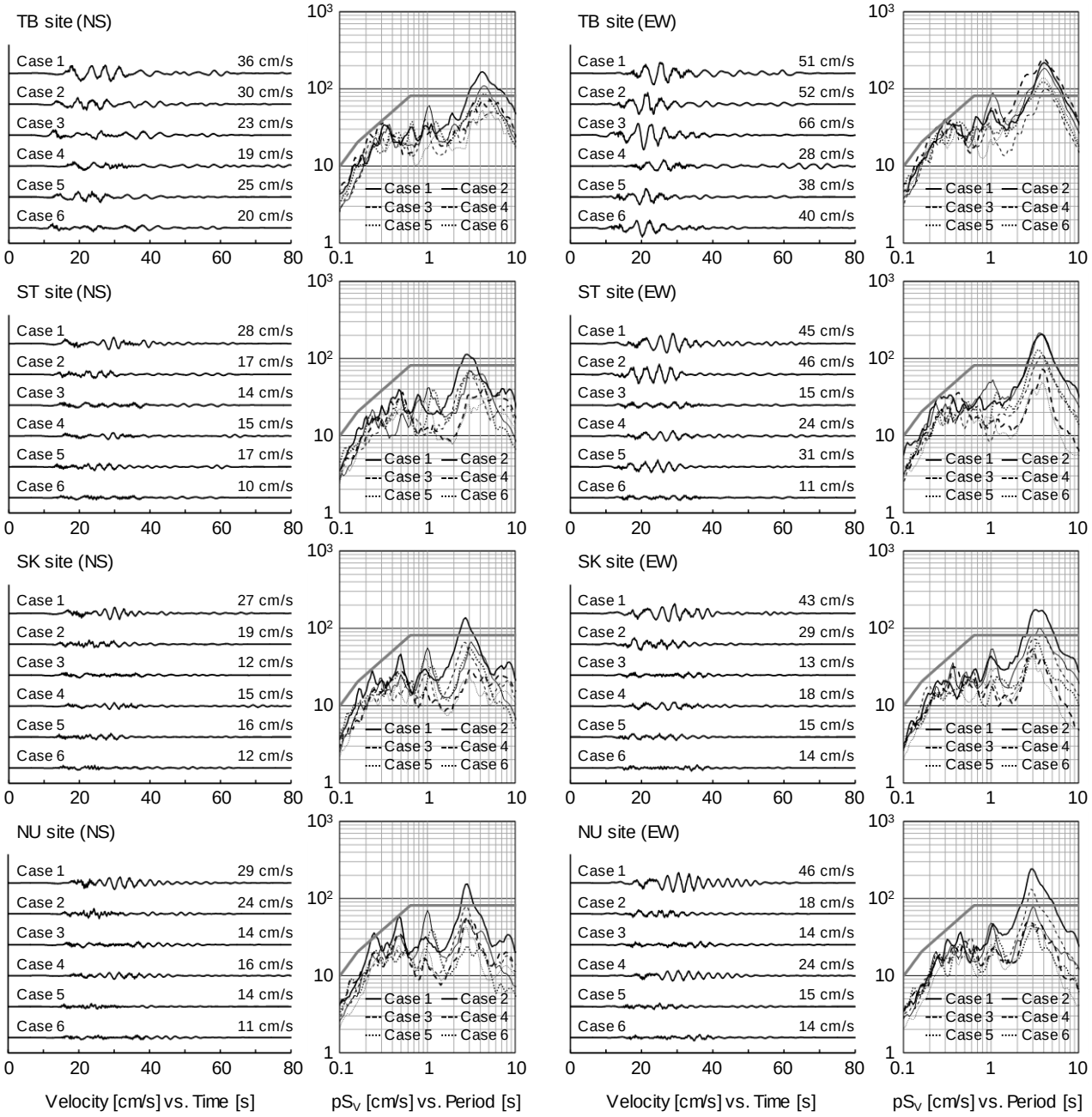

Fig. 3 – Ground motions at each site due to all cases of earthquake A.

The FDM calculation is carried out based on the Graves staggered grid method [11] and Levander's formulation of fourth order difference [12]. The grid is a cubic one whose grid size is 150 m at depths less than 15 km from the surface and 450 m elsewhere. The boundary at the depth of 15 km is treated using the method of Aoi and Fujiwara [13]. The effective period is greater than 1.9 s. The non-reflecting boundary condition of Clayton and Engquist [14] and the energy-absorbing boundary condition of Cerjan et al. [15] are applied to the edges of the model.

3.2 Ground motions of earthquake A

Figure 3 shows the ground motions at each site due to all the cases of earthquake A. The response spectra for a damping coefficient of 5% are also shown in Fig. 3.

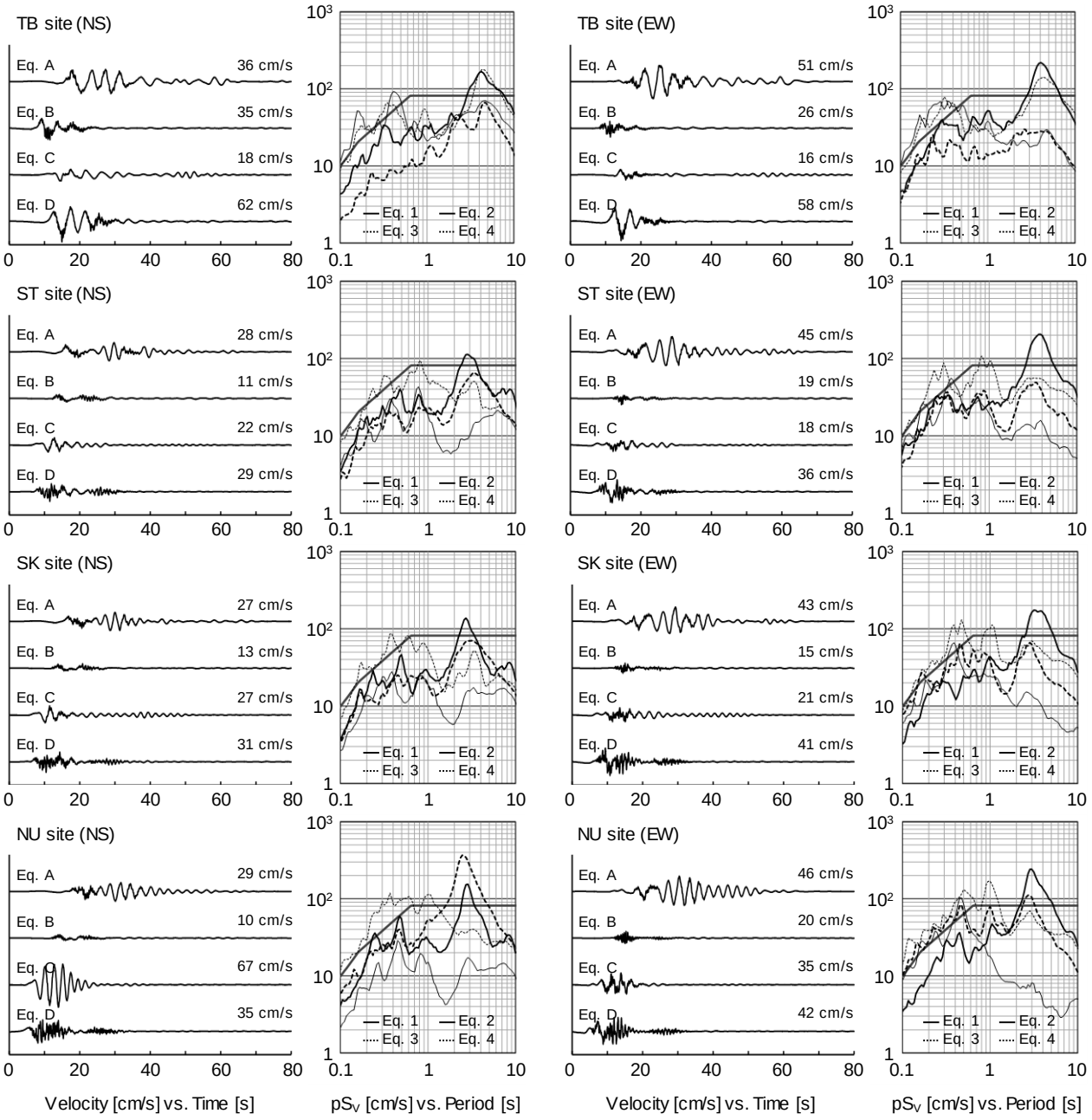

Fig. 4 – Ground motions at each site due to earthquakes A, B, C, and D.

According to the figure, the level of ground motion is largest in case 1. This reflects the fact that each site is located in the direction of fault rupturing. The fault rupture also proceeds toward the sites in case 4. However, the ground motion level is now marginally lower because the seismic moment of the near part of the seismic fault is smaller than that in case 1. The predominant periods seen in the response spectra are 4 s at site TB and 3 s at the other sites. The variation of the predominant period seems to correspond to the depth of the bedrock at each site. However, the predominant period at an individual site also differs according to the rupture case. The results in this section show that the predominant period of the ground motion could vary with respect to the asperity distribution and the rupture scenario. Similarly, it should be noted that the peak of the response spectrum is broad.

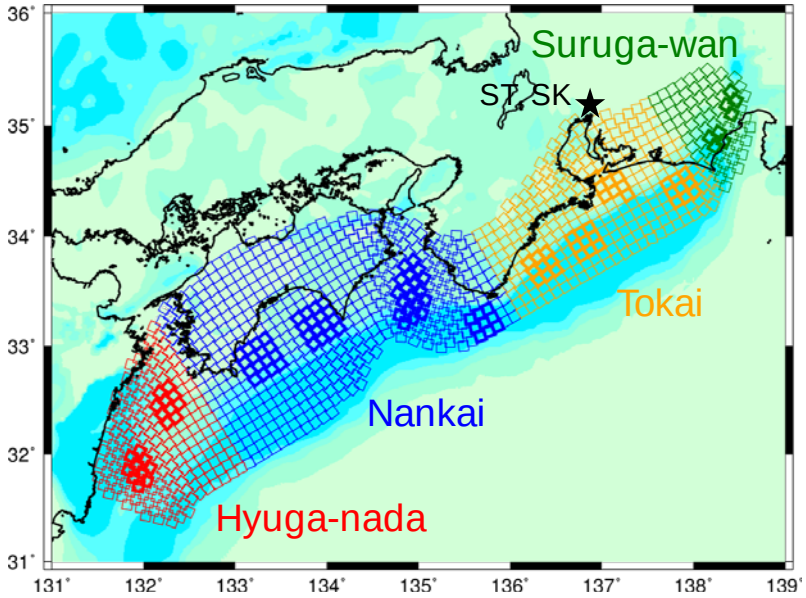

Fig. 5 – Soil structure of model area, ground motion prediction sites, and assumed seismic faults.

3.3 Ground motions by other earthquakes

Figure 4 shows the ground motions at each site due to earthquakes A, B, C, and D. For earthquake A, the ground motions are synthesized in case 1. The response spectra for a damping coefficient of 5% are also shown in Fig. 4.

According to the figure, the maximum velocities and the durations are largest for earthquake A. The NS component of the ground motion due to earthquake C is very large at site NU. Since the EW component of the ground motion contains a high-frequency wave at the same time, the large velocity in the NS component seems to be caused by the body wave. Site NU is located on the extended line of seismic fault C, so that the S wave is radiated strongly forward site NU. Compared with site NU, the main motions of the ground motion due to earthquake C at the other sites are smaller, while the coda part at the other sites is larger. In contrast, the coda part of the ground motion is the largest at site NU in the case of earthquake A. These effects are caused by the thick sedimentary layer beneath the Nobi Plain.

As seen in the response spectra in Fig. 4, the predominant periods of the ground motions are 4–5 s at site TB, and approximately 3 s at the other sites. However, these peaks vary in the range of approximately 1 s. This variation range is greater than that in the response spectra in Fig. 3. Therefore, the ground motion is affected not only by the asperity distribution and the rupture propagation but also by the complex soil structure in the propagation path. In relation to building design, we note that the response spectrum of the ground motion at sites on a sedimentary basin could have broad peaks, in addition to a predominant period.

4. Application to interplate earthquakes

4.1 Soil structure and seismic source model

In this section, the ground motion prediction method described in this paper is applied to an anticipated Nankai Trough earthquake. This is considered to be one of the most serious potential interplate earthquakes around Japan. Figure 5 shows the soil structure of the model area, the ground motion prediction sites, and the assumed seismic faults. The soil structure is represented as the distribution of the upper depth of the layer with V_S = 3200 m/s, as in Fig. 3. Although four cases of the distribution of the strong motion generation area (SMGA) are assumed by the Central Disaster Management Council of Japan [16], only the basic case is used in this paper because of limitations of space. The source region is divided into four parts from the west, namely the areas of Hyuga-nada, Nankai, Tokai, and Suruga-wan.

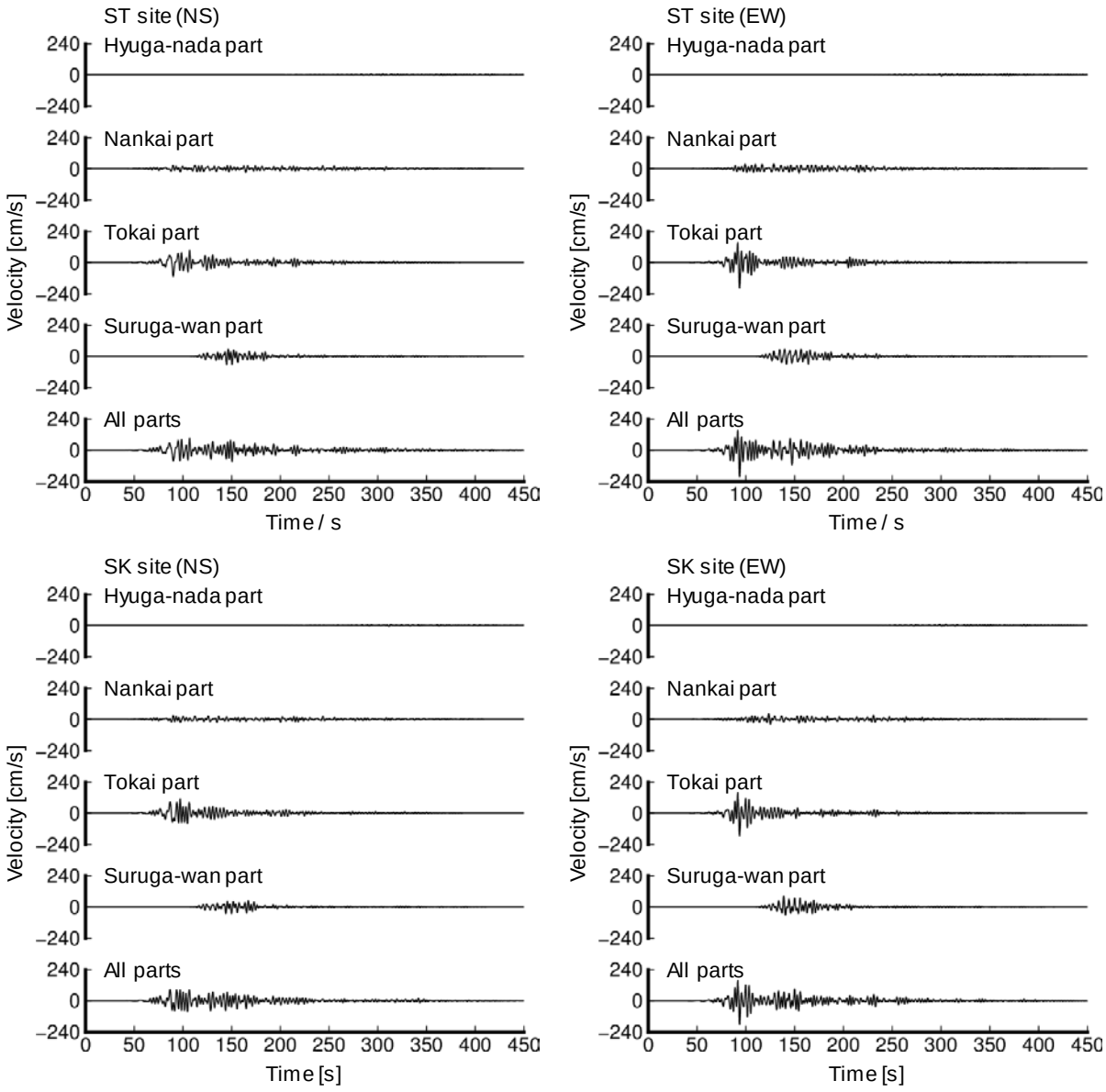

Fig. 6 – Ground motions at each site due to individual parts and an entire Nankai Trough earthquake.

4.2 Predicted ground motions of a Nankai Trough earthquake

Figure 6 shows the ground motions at each site due to individual parts and an entire Nankai Trough earthquake. The contribution of the Tokai part is the largest at both sites and in both components. In contrast, the contribution of the Hyuga-nada part is almost negligible. These results reflect the distance between the seismic source and each site. The ground motion due to the Suruga-wan part has a moderate amplitude, whereas that due to the Nankai part has a moderate duration time. Reflecting these contributions by each part, there are several wave groups in the ground motion due to the entire seismic fault. The ground motions at sites ST and SK are almost the same. However, they differ slightly in relation to the peak amplitude of the impulsive motion of the main part, even though these two sites are about 2 km apart. This difference may be due to the local irregularity of the soil structure.

Large interplate earthquakes, such as a Nankai Trough earthquake, often have complicated slip distributions. In such cases, it is hard to predict the ground motions for all assumed rupture scenarios. The ground motion prediction method described in this paper may be used efficiently in such cases. A Nankai Trough earthquake is an example of such an application. Since the results presented here for a Nankai Trough earthquake are preliminary ones, we intend to study them in more detail presently.

5. Conclusions

In this paper, we proposed an efficient method for predicting the long-period ground motions due to many possible earthquakes for a specific site. In general, long-period ground motion can be calculated accurately using the finite difference method (FDM) based on the soil structure model. However, ground motion prediction using FDM requires substantial computational resources. Here, we reduced the computational costs by using the reciprocity theorem to calculate Green's functions. The method was applied to predict the long-period ground motion at several sites in central Japan due to a few inland and interplate earthquakes. According to the results, the method is useful for predicting the ground motions at a specific site due to many seismic sources and rupture scenarios. In the future, the long-period ground motion at an important site will be predicted efficiently for any earthquake, accompanied by production of a database of Green's functions.

6. Acknowledgements

This work was supported by JSPS KAKENHI Grant Number 15K18151. Some of the figures in this paper were drawn using Generic Mapping Tools (GMT) [17].

7. References

[1] Trifunac MD, Hudson ED (1971): Analysis of the Pacoima Dam Accelerogram - San Fernando, California earthquake of 1971. *Bull. Seism. Soc. Am.*, **61**, 1393-1411.

[2] Boore DM (1972): A note on the effect of simple topography on seismic SH waves. *Bull. Seism. Soc. Am.*, **62**, 275-284.

[3] Bouchon M (1973): Effect of topography on surface motion. *Bull. Seism. Soc. Am.*, **63**, 615-632.

[4] Sánchez-Sesma F, Chávez-Pérez S, Bravo MA, Pérez-Rocha LE (1988): The Mexico earthquake of September 19, 1985 - On the seismic response of the valley of Mexico. *Earthquake Spectra*, **4**, 591-608.

[5] Building Research Institute: BRI Strong Motion Observation. http://smo.kenken.go.jp (2016.5.14 referred).

[6] Yuzawa Y, Nagumo H (2012): Factors of Variability and Measures for the Shakeability of Long-Period Ground Motion - Kanto Basin as an Example -. *Journal of Japan Association of Earthquake Engineering*, **12**, 41-59 (in Japanese).

[7] Terashima Y, Takahashi H, Fukuwa N, Mori M (2012): Study of Resonance between High-rise Buildings on Sedimentary Plain and Long-period Ground motions: Part.1 Analysis of Ground Motion Characteristics and Strong Motion Prediction in Osaka Basin. *Proceedings of 2012 Annual Meeting of Architectural Institute of Japan*, **B-2**, 151-152 (in Japanese).

[8] Simuté S, Fichtner A (2015): Seismic source inversion using Green's reciprocity and a 3-D structural model for the Japanese Islands, *American Geophysical Union, Fall Meeting 2015*, S23C-2727.

[9] Boore DM (1983): Stochastic simulation of high-frequency ground motions based on seismological models of the radiated spectra. *Bull. Seism. Soc. Am.*, **73**, 1865-1894.

[10] National Research Institute for Earth Science and Disaster Resilience: Japan Seismic Hazard Information Station, http://www.j-shis.bosai.go.jp/map/?lang=en (accessed 2016.5.14).

[11] Graves RW (1996): Simulating seismic wave propagation in 3D elastic media using staggered-grid finite differences. *Bull. Seism. Soc. Am.*, **86**, 1091-1106.

[12] Levander AR (1988): Fourth-order finite difference P-SV seismograms. *Geophysics*, **53**, 1425-1436.

[13] Aoi S, Fujiwara H (1999): 3D finite-difference method using discontinuous grids. *Bull. Seism. Soc. Am.*, **89**, 918-930.

[14] Clayton R, Engquist B (1977): Absorbing boundary conditions for acoustic and elastic wave equations. *Bull. Seism. Soc. Am.*, **67**, 1529-1540.

[15] Cerjan C, Kosloff D, Kosloff R, Reshef M (1985): A non-reflecting boundary condition for discrete acoustic and elastic wave equations. *Geophysics*, **50**, 705-708.

[16] Central Disaster Management Council of Japan (2012): http://www.bousai.go.jp/jishin/nankai/model/pdf/20120829_2nd_report5.pdf (accessed 2016.5.14).

[17] Wessel P, Smith WHF, Scharroo R, Luis JF, Wobbe F (2013): Generic Mapping Tools: Improved version released. *EOS Trans. AGU*, **94**, 409-410.